

In Vivo Micro-Imaging Using Alternating Navigator Echoes With Applications to Cancellous Bone Structural Analysis

Hee Kwon Song and Felix W. Wehrli*

In micro-magnetic resonance imaging of cancellous bone architecture, involuntary subject motion even on a sub-millimeter scale is detrimental and generally precludes accurate quantification of architectural parameters. In this work a navigator-assisted three-dimensional spin-echo technique is described and evaluated for imaging at 137 μm resolution in humans. The method is based on gradient navigator echoes following the spin-echo readout for sensing translational displacements alternately in x- and y-directions with a spatial resolution of 273 μm and a temporal resolution of 0.2 sec. The technique is shown to improve micro-images of the distal forearm significantly and to enhance accuracy and reproducibility of bone volume fraction, transverse contiguity, and tubularity, parameters introduced in prior work to characterize the trabecular network. It is further shown that a fourfold reduction in navigator sampling time, along with zero-filling, improves the accuracy of the navigator correction while reducing the minimum pulse repetition time or gradient heating. The data indicate that navigator-assisted micro-imaging is capable of effectively correcting sub-millimeter displacements in micro-imaging. Magn Reson Med 41:947–953, 1999. © 1999 Wiley-Liss, Inc.

Key words: navigator echoes; high-resolution imaging; motion correction; trabecular bone

Advances in nondestructive imaging of tissue microstructure have significantly furthered our understanding of the function and physiology of connective tissues. Among the technologies suited for imaging at resolutions on the order of 100 μm or better, NMR micro-imaging is unique in that it permits control of tissue contrast (1). However, much of the work reported so far on imaging of the microarchitecture of tissues such as cartilage (2,3) and cancellous bone (4–6) has been *ex vivo* on small specimens at high magnetic field. More challenging but also potentially medically more relevant is the ability to resolve microstructure *in vivo* in laboratory animals and humans. Besides signal-to-noise ratio (SNR), one of the most critical limiting factors *in vivo* is blurring from involuntary subject or physiologic motion, since a displacement even of a fraction of a millimeter could significantly degrade image quality. This problem is exemplified in a recent study in which micro-imaging was used for quantifying changes in cancellous bone structure in osteoporotic subjects: one-third of the data could not be analyzed due to blurring, presumably

from patient motion (7). Therefore, preventing or correcting for motion during the scan is a crucial prerequisite for achieving the resolution limited by voxel size and point-spread function. Immobilization alone is usually insufficient, and other methods may be needed.

One motion correction technique dealing with rigid-body motion involves collection of an additional set of data at each phase-encoding view, and using these projection data to correct for translational motion. The method of navigator echoes, first conceived by Ehman and Felmlee, has been used successfully for respiratory motion (8); the idea was later extended to correction of translational (9) and rotational motion (10) in diffusion-weighted imaging experiments.

In this work, a motion correction technique based on alternating navigator echoes for two-dimensional (2D) motion sensing was designed and implemented in a short-TR 3D pulse sequence for micro-imaging at $137 \times 137 \mu\text{m}^2$ pixel size. One of the specific goals was to evaluate the effectiveness of the technique in enhancing the accuracy of architectural parameters in the cancellous bone of the distal radius. A second goal was to test the feasibility of collecting a reduced number of navigator sample points without compromising motion detection accuracy. Shorter navigator readout is desirable for short-TR, 3D high-resolution sequences, in which collection of additional high-resolution projection data undesirably prolongs TR or when gradient duty-cycle limits are approached.

MATERIALS AND METHODS

Motion Detection and Data Analysis

Navigator echo motion detection was incorporated into a 3D fast large-angle spin-echo (FLASE) sequence (11) as depicted in Fig. 1. This sequence was chosen for trabecular bone imaging for several reasons. First, a fast 3D sequence is demanded by the need to obtain multiple thin slices to determine 3D structure accurately in a clinically practical scan time. Second, a spin-echo sequence was chosen to reduce spin dephasing from field inhomogeneities due to bone marrow susceptibility difference, causing blurring at the trabecular bone marrow interface (11,12).

Several modifications to the original navigator design were necessary for compatibility with the FLASE sequence. First, the navigator signal chosen was a gradient-echo collected immediately after the conventional spin-echo readout and rephasing of the phase- and slice-encoding gradients, since the ordinarily used spin-echo navigator will cause additional spin saturation in short-TR sequences such as FLASE. Alternatively, excitation of a separate slice for navigator signal acquisition had to be discounted since FLASE's 180° hard pulse would effectively saturate the regions outside the imaging slice. Further-

Department of Radiology, University of Pennsylvania Medical Center, Philadelphia, Pennsylvania.

Grant sponsor: NIH; Grant numbers: RO1 41443 and 40671.

A preliminary account of part of the present work was given at the ISMRM Sixth Scientific Meeting, Sydney, Australia, 1998.

*Correspondence to: Felix W. Wehrli, Department of Radiology/1 Founders, 3400 Spruce Street, Philadelphia, PA 19104.

E-mail: wehrli@oasis.rad.upenn.edu

This paper was reviewed through the office of an Associate Editor.

Received 13 October 1998; revised 8 December 1998; accepted 4 January 1999.

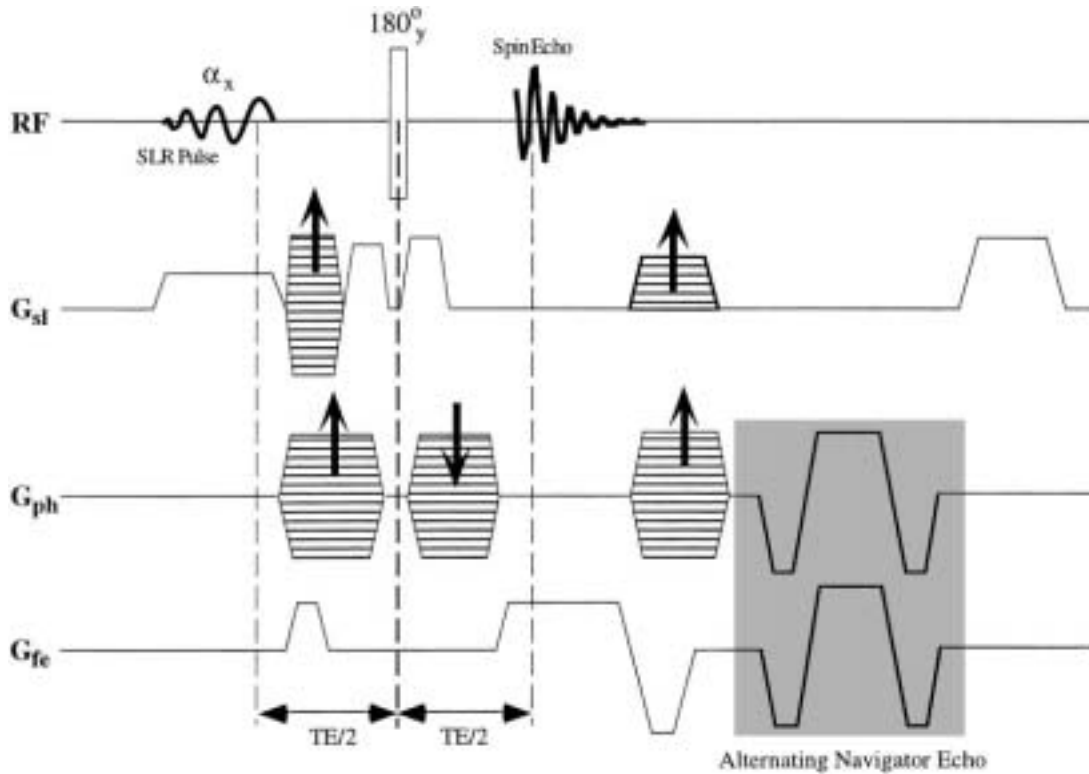


FIG. 1. FLASE sequence with alternating navigator echoes. Collection of navigator data alternated between frequency and phase-encoding axes. The zeroeth moments of all three gradients are nulled before the navigators are acquired. Also, to maintain steady state, the navigator gradients are refocused after collecting motion data.

more, to determine displacements along both x - and y -axes (in-plane), navigator echoes had to be alternated between these two directions. Although both x - and y -navigators could have been collected sequentially at each phase-encoding step, this option would cause additional T_2^* dephasing at the second navigator echo position. Since the TR used in these studies was typically less than 100 msec, alternating the navigator between the two orthogonal directions still provided positional information at a rate of about 5/sec along each direction. Since slice thickness was considerably greater than in-plane pixel size, and motion is less likely along the inferior-superior direction, motion was not compensated for along the z -direction.

A one-dimensional projection of the object is found by Fourier transforming the navigator echo signal, which is then compared with a reference position to determine the shift. Wang et al (13) found that least-squares methods were more reliable for determining shifts in the presence of noise than correlation or edge-detection algorithms. The least-squares approach involves minimization of the residual $R(d)$ defined as:

$$R(d) = \sum_x [p(x-d) - p_r(x)]^2 \quad [1]$$

where $p(x)$ is the current navigator projection, $p_r(x)$ is the reference projection, which can be arbitrarily chosen from any one of the projections, and summation is over the entire profile. The value of d at which $R(d)$ is a minimum corresponds to the amount the current view needs to be shifted relative to the reference. A least-squares technique

was used to determine shifts for alternate views on each axis, and the missing views were determined by linear interpolation. After motion was determined for each view, an averaging filter with a width of five views was applied to smooth out some of the artifactual, abrupt changes in detected motion caused by noise. Although this low-pass filtering causes some loss in temporal sensitivity, it still allows for motion resolution of less than half a second, which is sufficient in most applications, in which high-frequency fluctuating movements are absent. Measured displacements (x_d, y_d) for each line of k -space were then used to correct the phase of the signal according to the equation:

$$S_c(k_x, k_y) = S(k_x, k_y) \cdot e^{-j2\pi(k_x(x_d/N_x) + k_y(y_d/N_y))} \quad [2]$$

where S_c is the corrected signal, S is the detected signal, and N_x and N_y are number of points collected along x and y directions, respectively.

After motion compensation, parameters characterizing the trabecular network, bone volume fraction (BVF), transverse contiguity (TCon), and tubularity (Tub) (5) were calculated using the methods briefly described below. First, BVF maps were generated by a histogram deconvolution technique as described in ref. 7. Each point on the BVF maps represents the probability of containing bone, i.e., it expresses the fraction of the voxel that is occupied by bone. From this map, two other parameters can be extracted, TCon and Tub, which are essentially spatial autocorrelations of the BVF maps, in the transverse and longitudinal

directions, respectively (5):

$$TCon = \frac{\langle BVF(x,y,z_1)BVF(x + n_x,y + n_y,z_1) \rangle_{x,y,n_x,n_y}}{\langle BVF(x,y,z_1)BVF(x,y,z_1) \rangle_{x,y}} \quad [3]$$

$$Tub = \frac{\langle BVF(x,y,z_1)BVF(x,y,z_1 + 1) \rangle_{x,y}}{\langle BVF(x,y,z_1)BVF(x,y,z_1) \rangle_{x,y}} \quad [4]$$

where $\langle \rangle_{x,y}$ indicates a spatial average over all pixel locations (x,y) within slice z_1 and $\langle \rangle_{x,y,n_x,n_y}$ over all (x,y) points, as well as over n_x and n_y where $n_x, n_y = -1, 0, \text{ or } 1$, except for the case when both $n_x = 0$ and $n_y = 0$. According to the two equations, TCon and Tub describe the normalized “contiguity” of bone structures in the transverse and longitudinal directions, respectively, and are measures of structural integrity.

In Vivo Experiments

The right distal radius of a 29-year-old volunteer was imaged using a small quadrature birdcage coil built specifically for microimaging of the wrist. The scan was performed twice, first while the subject was instructed to remain as motionless as possible (control), and again while the subject was making voluntary movements during the scan. The following parameters were used: TR/TE 80/7.8 msec; 7 cm field of view (FOV), 0.5 mm thick; $512 \times 256 \times 32$ matrix ($137 \times 137 \times 500 \mu\text{m}^3$ resolution); 140° flip angle, ± 16 kHz bandwidth, scan time 10.9 min. Additionally, a 56-year-old woman was imaged at $137 \times 137 \times 350 \mu\text{m}^3$ resolution, with similar parameters as above,

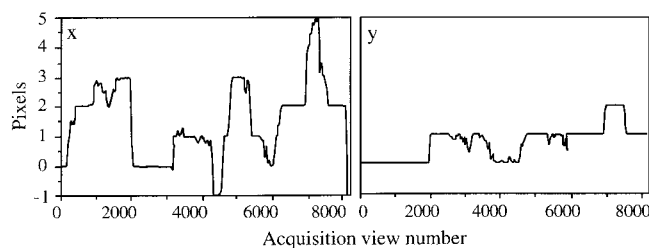


FIG. 2. Motion along x and y directions in acquired order shown in pixels. A five-view smoothing window was applied to reduce artifactual spurious motion caused by noise. Five pixels correspond to approximately $700 \mu\text{m}$.

except for ± 8 kHz bandwidth and TE 9.7 msec. With these parameters, the period between the spin-echo and the navigator echo was approximately 18 msec at ± 16 kHz and 30 msec at ± 8 kHz. The patient in this case was told to remain as motionless as possible. Data were reconstructed and structural parameters derived before and after correcting for motion by methods described above. For these studies, to reduce the navigator readout time, navigator FOV was set to twice that of the image, and bandwidth was fixed at ± 32 kHz. It will be demonstrated with simulations that reducing the resolution of navigator data does not compromise motion accuracy if zero-filling is used.

To test the reproducibility of the motion correction scheme, four consecutive scans were performed in a 25-year-old female volunteer with the same parameters as above ($137 \times 137 \times 350 \mu\text{m}^3$). The subject was told to remain as motionless as possible, and scans were per-

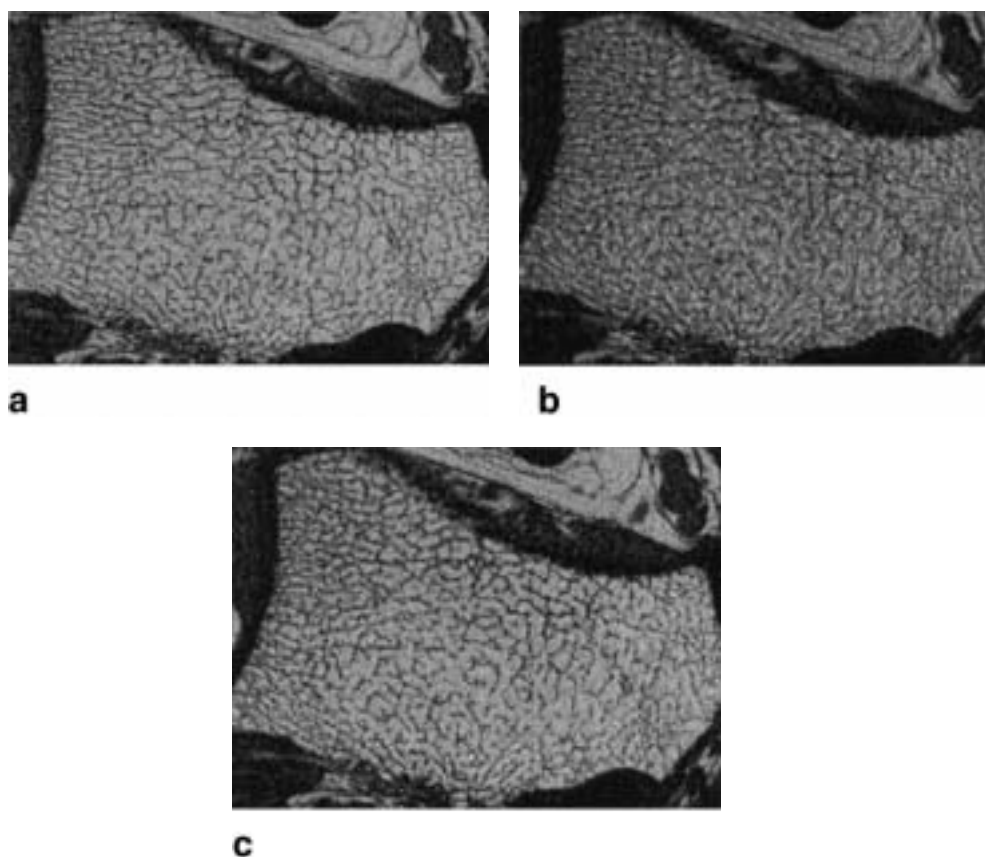


FIG. 3. Control (a), motion-corrupted (b), and-corrected (c) images of the distal radius of a 29-year-old volunteer, showing improvements in image quality after motion compensation via gradient navigator echoes. Individual trabeculae are more easily identified after motion correction (c) than before correction is applied (b). Image resolution is $137 \times 137 \times 500 \mu\text{m}^3$, and only the most pertinent regions of the images are displayed.

Table 1
Structural Parameter Comparisons With and Without Motion
and After Motion Compensation

	BVF	Tub	TCon
Control	0.152	0.590	0.570
Corrected	0.154	0.597	0.576
Motion corrupted	0.134	0.555	0.544
Corrected	0.144	0.571	0.570

formed without repositioning, with about 2 min pauses between scans. Structural parameters were computed before and after motion correction and results compared. All experiments were performed on a GE Signa 1.5 T whole-body system with Epic 5.6 configuration and Echospeed gradients.

Computer Simulations

Intuition would imply that displacement accuracy be limited by the pixel resolution of the navigator projections, since an integer number of pixels are shifted and compared with the reference projection. It should be possible, however, to determine motion with even greater accuracy than the pixel resolution by interpolating between the original points. Alternatively, navigator projections with lower resolutions can be collected and interpolated to image pixel resolution, before motion information is calculated. A computer simulation was performed to test this hypothesis. Various amounts of noise and positional shifts were applied to a simulated profile consisting of circular and

rectangular projections, and detected motion was compared with and without zero-filling the outer regions of its k-space.

RESULTS AND DISCUSSION

Figure 2 shows the navigator-detected motion from the second session (with voluntary motion), and Fig. 3 compares the control, motion-corrupted, and motion-corrected images. Blurring is obvious in motion-corrupted images, and significant improvement is seen after correction. Table 1 shows that the measured parameters are incorrectly estimated when motion is present and that they can be improved by motion correction using navigator echoes. It is assumed that in the absence of motion true BVF is obtained, an assumption that is justified on the basis of the work in ref. 14, in which it is demonstrated that for $\text{SNR} > 8$ the error in calculated BVF is < 0.01 . Furthermore, the data in Table 1 show that motion correction applied to the control image only insignificantly affects the structural parameters.

Pre- and post-motion compensated images from the 56-year-old female volunteer are shown in Fig. 4. The measured structural parameters for this subject are listed in Table 2. Although the subject was instructed to remain as motionless as possible, blurring is obvious in the acquired images before motion correction. At an in-plane resolution of $137 \mu\text{m}$, avoiding motion on a scale of the order of the pixel size is virtually impossible, even when immobilizing the wrist and arm. Navigator motion correction clearly was

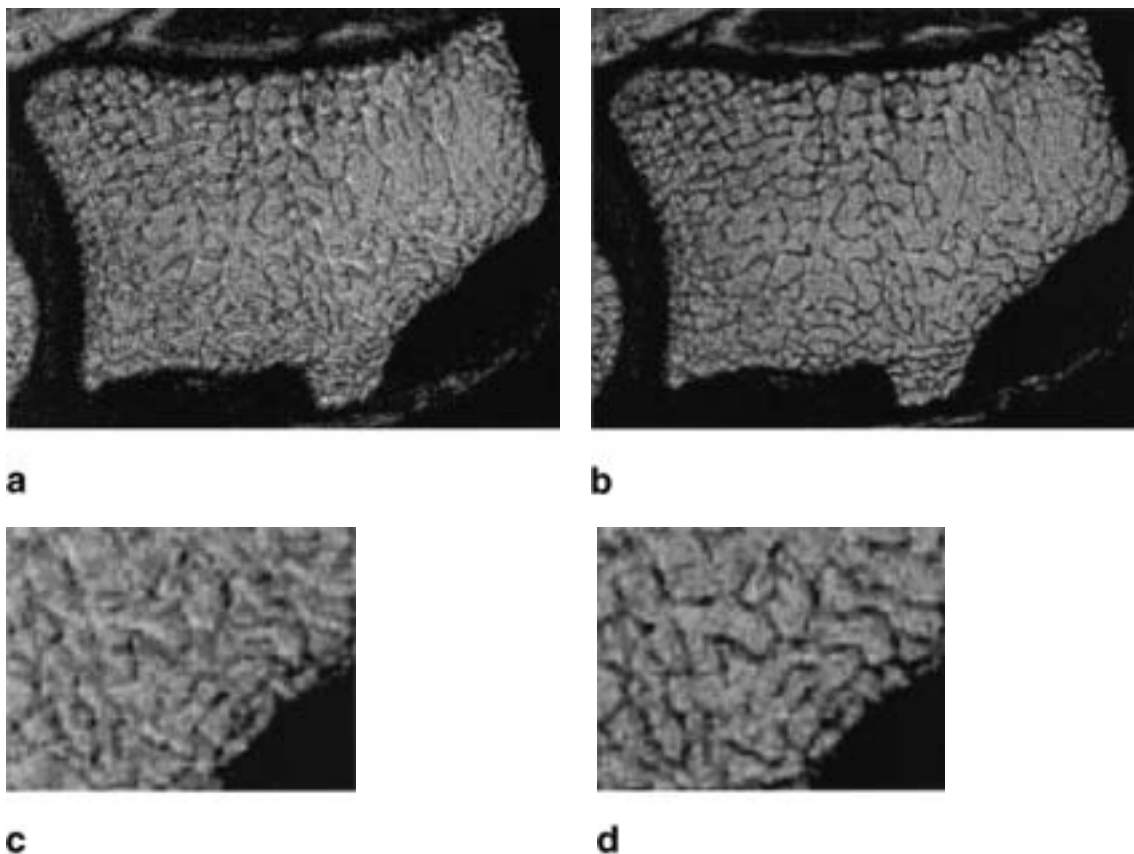


FIG. 4. Images of the distal radius from a 56 year-old woman at $137 \times 137 \times 350 \mu\text{m}^3$ voxel size, before (a) and after (b) motion correction. c, d: $2\times$ magnifications of the lower right portions of a and b, respectively.

Table 2
Measured Structural Parameters Before and After Motion Compensation for the 56-Year-Old Volunteer*

	BVF	Tub	TCon
Before correction	0.106	0.581	0.564
After correction	0.114	0.628	0.583

*The subject remained as motionless as possible.

able to improve image quality dramatically, allowing individual trabeculae to be more easily discerned.

As the data demonstrate, gradient navigator echoes provide sufficient signal (despite T_2^* decay) to detect sub-millimeter displacements. Gradient echo navigators are indicated for short-TR imaging, for which a separate excitation may not be possible or desirable. Also, unlike using a separate slice for collecting navigator information, this motion-sensing strategy has the advantage of collecting displacement information from the same location as the image slice without increasing imaging time. Exciting a separate slice is also precluded if the imaging volume occupies the entire sensitive region of a local receiver coil.

Displacements along both in-plane axes could in theory be measured with just one navigator echo by applying a small constant phase-encoding gradient along the second direction. However, this method was ruled out since intraview motion along any of the three axes can cause constant phase shifts, which would be misinterpreted as a simple y -displacement (8,15). Alternatively, both x and y navigator echoes could have been collected for every view by sequentially acquiring two separate orthogonal echoes (15,16). However, given the short TR used in this study (80 msec), it was deemed unnecessary since very rapid motion was unexpected. Collecting only one navigator echo per view also reduces the memory size required to store and process the already large amount of data (32 MB per image set, with one navigator echo per view).

The data in the repeat study, summarized in Table 3, indicate a significant reduction in the standard deviation (from 0.004 to 0.001). A clinically relevant change in BVF is on the order of 3–5% which, at a BVF of 0.15, amounts to 0.0045–0.0075. The data thus suggest that detection of such small changes may be feasible. Because averaging many slices tends to mask actual parameter differences between individual slices, BVF measurements from the first two scans were also compared on a slice-by-slice basis. The resulting plot (Fig. 5) more clearly demonstrates the increased precision after correction. Ideally, the points should lie on a straight line with a slope of unity. The data clearly show an increase in the strength of the correlation after navigator correction.

For the simulation experiment designed to test the accuracy of the navigator echo technique to compensate for rigid-body motion, a computer-generated phantom was

Table 3
Averages and Standard Deviations (in Parentheses) of Bone Parameters Acquired From Four Scans Before and After Compensating for Motion*

	BVF	Tub	TCon
Before correction	0.115 (0.004)	0.569 (0.015)	0.503 (0.004)
After correction	0.117 (0.001)	0.578 (0.004)	0.505 (0.003)

*The subject was instructed to remain as motionless as possible.

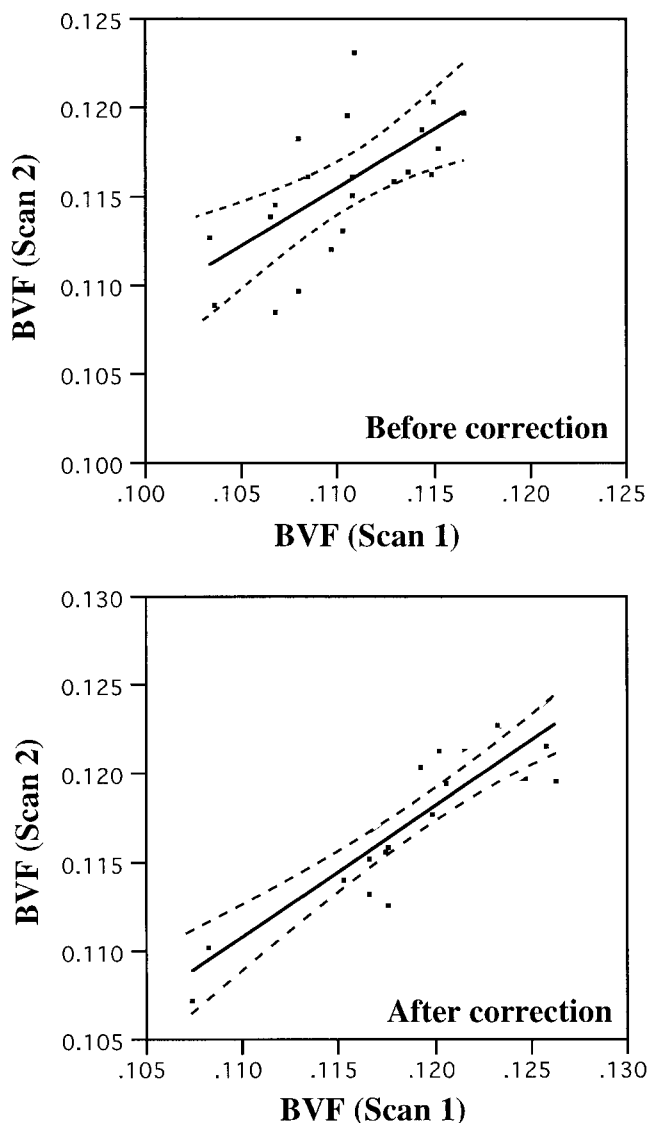


FIG. 5. Slice-by-slice BVF comparison for two consecutive scans from a reproducibility study. The R^2 values before and after motion correction were 0.43 and 0.79, respectively. The dotted lines represent the 95% confidence intervals of the slope. The slope and y -intercept of the fit were 0.65 and 0.044, respectively, before correction, and 0.74 and 0.030 after. Ideally, the slope should be 1 and the intercept 0.

first shifted by integer increments from -10 to 10 pixels, followed by addition of varying amounts of complex noise such that SNR, defined as peak signal divided by standard deviation of noise in each channel, was 4, 6, 8, 10, or 12. The simulated profile consisted of projections of a circle and a square, created first in k -space using Bessel and sinc functions, respectively, and Fourier transformed into image space. Figure 6a and b shows simulated projections before and after noise was added for SNR = 10. Noisy profiles were then transformed back into k -space, and outer regions were zero-filled (ZF) by a factor of 4 or 16 and transformed into image space. A zero-fill factor of 4 means that only the central one-fourth of the signal was kept and the rest zero-filled; ZF = 16 means that only the central $1/16$ was not zeroed. These two cases are shown in Fig. 6c and d for SNR = 10. For each of the shifted, noisy profiles, least-squares fitting was used to determine the displace-

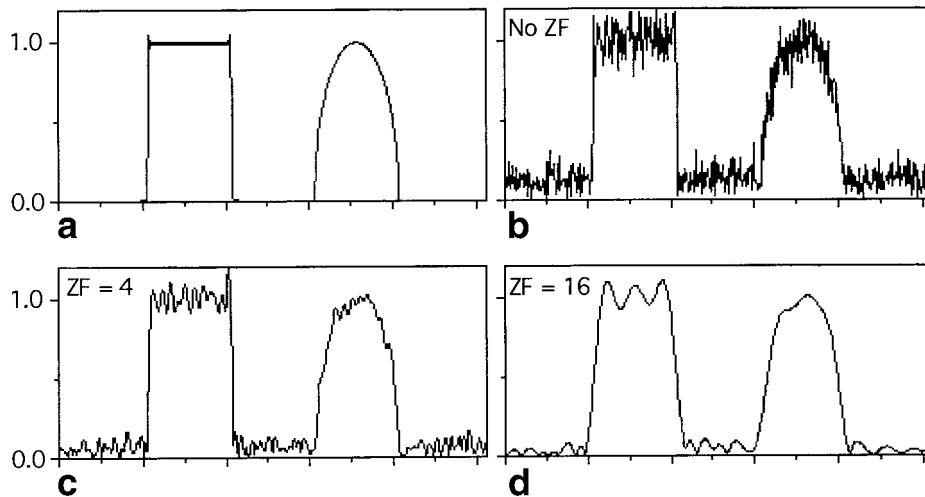


FIG. 6. Profile comparison for SNR = 10. **a:** Profile before noise was added. **b:** Profile using all 512 points of k-space signal (no ZF). **c:** ZF = 4. **d:** ZF = 16. Notice that, as expected, projections become less noisy with increasing ZF, but high-frequency boundary information is also lost.

ments, using noisy, but unshifted reference profiles (which were similarly zero-fill processed).

Figure 7 compares the results from the simulation experiments showing, as expected, that positional accuracy improves with increasing SNR. The plots also show that despite the lower resolution projections (reduced by up to a factor of 16), single-pixel shifts can be reliably detected by zero-filling the signal to the desired resolution. In fact, a lower number of acquired data samples, followed by zero-filling, may produce more accurate results, which is demonstrated with the center plot (ZF = 4), showing improved agreement between actual and detected displacement relative to ZF = 1. This finding is probably the result of increased SNR in the profiles (Fig. 6), since no noise is collected from the outer k-space regions.

The effectiveness of a reduced number of data samples for the navigator signal, along with zero-filling, can be understood by considering that, in principle, for rigid-body motion, only two data points are necessary to determine the translational displacement to arbitrary precision, since only two points are required to fit an MR signal to a linear phase shift function. This, however, is precisely the situation for translational motion. In practice, of course, more points need to be collected to ensure accurate phase

determination in the presence of noise. In the present study, lower resolution navigators were sufficient to determine single-pixel shifts by first interpolating to the proper “resolution” (by means of zero-filling in the spatial frequency domain). The results also indicate that it is possible to determine sub-pixel shifts (smaller than the image resolution), simply by zero-filling to higher resolutions.

As mentioned above, linear fitting of the phase difference between two navigator signals also allows the determination of positional shifts. This method also requires much less time than the correlation methods. It was found, however, that in this work, there are phase errors in the navigator signal that cause errors when linear fitting is attempted. Phase inconsistencies may be due to strong T_2^* decay arising from prolonged gradient echo times or to the view-to-view differences of phase- and slice-encoding gradients between the initial RF pulse and navigator echo during each TR. Although these encoding gradients are eventually rewound before motion data are collected, non-linearities in gradient amplifiers or differences in eddy currents can introduce the phase errors.

Low-resolution navigators may be desirable to reduce the total data size, which can become rather large in high-resolution, 3D imaging experiments. This advantage

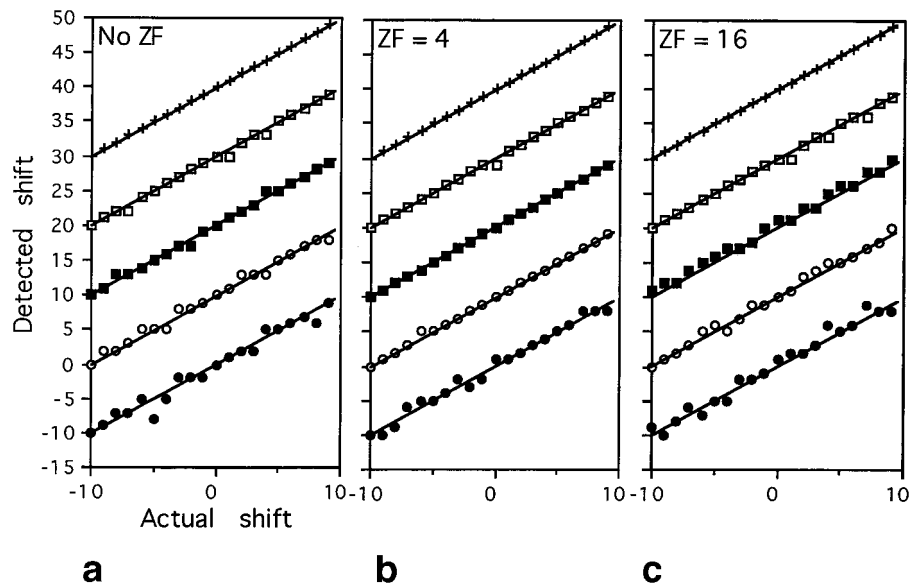


FIG. 7. Actual simulated versus detected shift assuming (a) no zero-filling (ZF), (b) ZF = 4, and (c) ZF = 16, where the ZF factor indicates that only 512/ZF central k-space points were used and the rest were zero-filled. Different markers are for different SNRs, increasing from bottom to top, 4, 6, 8, 10, and 12. Straight lines indicate true locations where points should lie. Data points for all SNRs except for SNR = 4 were offset for better visualization (i.e., all the straight lines should actually coincide with the lowest line, corresponding to actual displacements from -10 to +10 pixels).

becomes even more significant if multiple navigators are collected during each TR. Reduced navigator readout times can also allow for shorter TRs, or, alternatively, reduce gradient duty cycle and heating, which can potentially be a problem in high-resolution, short TR sequences.

CONCLUSIONS

Interest in MR imaging of tissue microstructure in various organ systems is currently growing. However, *in vivo* it is often neither the pixel size nor the point-spread function that determines the effective resolution, but rather motion, often subtle aperiodic subject motion. The severity of the problem becomes evident when one considers that at the resolution at which the current micro-imaging was conducted, a 1 mm displacement corresponds to seven pixels! Motion correction in micro-imaging therefore poses unique challenges in that the corrections needed demand an order of magnitude greater accuracy than is necessary in typical clinical imaging.

This work demonstrates that the use of gradient navigator echoes is effective and improves the estimation of structural parameters in microimaging. It has also been shown that navigator data with lower resolution can be used to correct for motion with greater accuracy than it normally would allow by zero-padding the navigator k-space signals before Fourier transforming into image space. The need for reducing navigator sampling time becomes more stringent as TR is shortened to reduce scan times, or as gradient duty cycle limits are approached. Finally, the use of motion compensation techniques such as the navigator method may be critical to achieve the accuracy needed for longitudinal studies, e.g., to detect changes in bone architecture in response to drug treatments.

ACKNOWLEDGMENTS

The authors thank Maria Seara and Drs. Masaya Takahashi and Jeffrey Hopkins for help in carrying out the experiments.

REFERENCES

1. Callaghan PT. Principles of nuclear magnetic resonance microscopy. New York: Oxford University Press; 1991.
2. Gründer W, Wagner M, Werner A. MR-microscopic visualization of anisotropic internal cartilage structures using the magic angle technique. *Magn Reson Med* 1998;39:376.
3. Gründer W, Kanowski M, Wagner M, Werner A. Visualization of pressure distribution within loaded joint cartilage by application of magic angle sensitive NMR microscopy. In: Proceedings of the ISMRM 6th Scientific Meeting, Sydney, Australia, 1998. p 405.
4. Chung H, Wehrli FW, Williams JL, Kugelmass SD, Wehrli SL. Quantitative analysis of trabecular microstructure by 400 MHz nuclear magnetic resonance imaging. *J Bone Miner Res* 1995;10:803–811.
5. Hwang SN, Wehrli FW, Williams JL. Probability-based structural parameters from 3D NMR images as predictors of trabecular bone strength. *Med Phys* 1997;24:1255–1261.
6. Kapadia RD, Majumdar S, Stroup GB, Hoffman SJ, Zhao H, Gowen M, Sarkar SK. Quantitative analysis of MR microscopy images of trabecular bone architecture in rat model of osteoporosis. In: Proceedings of the ISMRM 6th Scientific Meeting, Sydney, 1998. p 404.
7. Wehrli FW, Hwang SN, Ma J, Song HK, Ford JC, Haddad JG. Cancellous bone volume and structure in the forearm: noninvasive assessment with MR microimaging and image processing. *Radiology* 1998;206:347–357.
8. Ehman RL, Felmlee JP. Adaptive technique for high-definition MR imaging of moving structures. *Radiology* 1989;173:255–263.
9. Ordidge RJ, Helpert JA, Qing ZX, Knight RA, Nagesh V. Correction of motional artifacts in diffusion-weighted MR images using navigator echoes. *Magn Reson Imaging* 1994;12:455–460.
10. Anderson AW, Gore JC. Analysis and correction of motion artifacts in diffusion weighted imaging. *Magn Reson Med* 1994;32:379–387.
11. Ma J, Wehrli FW, Song HK. Fast 3D large-angle spin-echo imaging (3D FLASE). *Magn Reson Med* 1996;35:903–910.
12. Jara H, Wehrli FW, Chung H. High-resolution variable flip angle 3D MR imaging of trabecular microstructure *in vivo*. *Magn Reson Med* 1993;29:528.
13. Wang Y, Grimm RC, Felmlee JP, Riederer SJ, Ehman RL. Algorithms for extracting motion information from navigator echoes. *Magn Reson Med* 1996;36:117–123.
14. Hwang SN, Wehrli FW. Estimating voxel volume fractions of trabecular bone on the basis of magnetic resonance images acquired *in vivo*. *Int J Imaging Syst Technol* 1999;10:186–198.
15. Felmlee JP, Ehman RL, Korin HW, Riederer SJ. Measurement of multi-axis motion using NAV echoes. In: Proceedings of the ISMRM 8th Annual Meeting, Amsterdam, The Netherlands, 1989. p 68.
16. Butts K, de Crespigny A, Pauly JM, Moseley M. Diffusion-weighted interleaved echo-planar imaging with a pair of orthogonal navigator echoes. *Magn Reson Med* 1996;35:763–770.